A New 6-DOF Quadrotor Manipulation System: Design, Kinematics, Dynamics, and Control

Mohamed Fanni and Ahmed Khalifa

***Abstract*—The research on aerial manipulation has increased rapidly in recent years. In the previous work, a manipulator or a gripper is attached to the bottom of a quadrotor to facilitate the interaction with the environment. However, the previously introduced systems suffer from either limited end-effector degrees of freedom (DOF) or small payload capacity. In this paper, a quadrotor with a 2-DOF manipulator that has a unique topology to enable the end-effector to track a desired 6-DOF trajectory with minimum possible actuators is investigated. The proposed system is designed and modeled. However, such a system produces complexity in its inverse kinematics and control. A novel solution to the inverse kinematics problem is presented, which requires a solution of complicated algebraic/differential equations. Its accuracy is verified via numerical results. In order to solve the control problem, the system nonholonomic constraints are utilized with a model-free and low computation cost robust control technique. Moreover, the system stability proof under the proposed controller is carried out. A prototype of the proposed system is built and its design is verified via a flight test. In addition, the system feasibility and efficiency are enlightened.**

***Index Terms*—Aerial manipulation, disturbance observer, dynamic modeling, inverse kinematics, quadrotor.**

NOMENCLATURE

Σ_b	Robot body frame.
Σ	World-fixed inertial reference frame.
p_b	Position of body frame with respect to Σ.
R_b	Rotation matrix from body frame to world frame.
Φ_b	The triple ZYX yaw-pitch-roll angles.
Σ_e	Frame attached to the end-effector.
Θ	Vector of joint angles of the manipulator.
p_{eb}^b	Position of Σ_e with respect to Σ_b expressed in Σ_b.
p_e	The position of Σ_e with respect to Σ.
χ_e	The 6-degrees of freedom (DOF) operational coordinates.
q	The quadrotor/joint space coordinates.
Φ_e	Euler angles of the end-effector.
ω_b	Angular velocity of the quadrotor expressed in Σ.
ω_e	The angular velocity of Σ_e.
ω_{eb}^b	The angular velocity of the end-effector relative to Σ_b and is expressed in Σ_b.
v_{eb}^b	Generalized velocity of end-effector w.r.t Σ_b.
J_{eb}^b	The manipulator Jacobian.
v_e	The generalized end-effector velocity.
T_b	Transformation matrix between ω_b and $\dot{\Phi}_b$.
J	The system Jacobian.
ζ	Independent coordinate.
σ_b	The dependent coordinates.
χ_b	Quadrotor body coordinates.
τ_{m_i}	Torque acting on joint i.
$F_{m,q}^b$	Manipulator forces on the quadrotor in Σ_b.
$M_{m,q}^b$	Interaction moments.
$F_{m,q}$	Interaction forces expressed in the inertial frame.
M_i, N_i	Nonlinear terms of the manipulator dynamics.
m	The mass of the quadrotor.
τ_{a_i}	Input moments about the three body axes.
Ω_j	Angular velocity of rotor j; $j = 1, 2, 3, 4$.
F_j/M_j	Thrust force/Drag moment of rotor j.
K_{f_j}	Thrust coefficient of rotor j.
K_{m_j}	Drag coefficient of rotor j.
T	The total thrust applied to the quadrotor.
d	Length of the quadrotor arm.
$\overline{\Omega}$	Collective speed of the speed of the four rotor.
I_r	Rotor inertia.
I_i	Inertia of the vehicle around its body-frame.
M	Inertia matrix of the combined system.
C	Matrix of Coriolis and centrifugal terms.
G	Vector of gravity terms.
d_{ex}	Vector of external disturbances.
u	Vector of the actuator inputs.
B, N	Input and Control matrices.
H	Transforms the body input forces to Σ.
$\chi_{e,r}$	Reference trajectory for the end-effector pose.
r_{ij}	The ijth element of the rotation matrix R_e.
τ	Vector of the input generalized forces.
M_n	System nominal inertia matrix.
τ^{des}	Desired input to the robot.
g_i	Low-pass filter bandwidth of the ith variable of q.
P	Vector of g_is.
$Q(s)$	Matrix of the low-pass filter of disturbance observer (DOb).

Manuscript received July 18, 2016; revised October 29, 2016 and December 27, 2016; accepted March 4, 2017. Date of publication March 10, 2017; date of current version June 14, 2017. Recommended by Technical Editor M. O. Efe.

M. Fanni is with the Department of Mechatronics and Robotics Engineering, Egypt-Japan University of Science and Technology, New Borg El Arab 21934, Egypt, on leave from the Department of Production Engineering and Mechanical Design, Mansoura University, Mansoura 35516, Egypt (e-mail: mohamed.fanni@ejust.edu.eg).

A. Khalifa is with the Department of Industrial Electronics and Control Engineering, Faculty of Electronic Engineering, Menoufia University, Al Minufiyah 32952, Egypt (e-mail: ahmed.khalifa@el-eng.menofia.edu.eg).

Color versions of one or more of the figures in this paper are available online at http://ieeexplore.ieee.org.

Digital Object Identifier 10.1109/TMECH.2017.2681179

τ^{dis}	System extended disturbances.
$\hat{\tau}^{\mathrm{dis}}$	System estimated disturbances.
M_{n_a}	Nominal inertia for the translational coordinates.
M_{n_v}	Nominal inertia for the rotational coordinates.
$\dot{q}^{\mathrm{des}}$	Output from the outer loop controller.
e_v	Error of the DOb internal loop.
L_p	L_p space; $p = [1, \infty)$.
H_{PD}	Exponentially stable transfer function.

I. Introduction

QUADROTOR system is one of the unmanned aerial vehicles (UAVs), which offer possibilities of speed and access to regions that are otherwise inaccessible to ground robotic vehicles. However, most research on UAVs has typically been limited to monitoring and surveillance applications, where the objectives are limited to "look" and "search" but "do not touch." Due to their superior mobility, much interest is given to utilize them for aerial manipulation. Previous research on aerial manipulation can be divided into three approaches.

In the first approach, a gripper or a tool is installed at the bottom of a UAV to transport a payload or interact with existing structures. In [1]–[3], a quadrotor with a gripper is used for transporting blocks and to build structures. In [4], a force sensor is used to apply a normal force to a surface. Accordingly, not only the attitude of the payload/tool is restricted to the attitude of the UAV, but also the accessible range of the end-effector is confined due to the fixed configuration of the gripper/tool with respect to the UAV body and blades. Consequently, the resulting aerial system has four DOF, three translational DOF, and one rotational DOF (Yaw), i.e., the gripper/tool cannot possess pitch or roll rotation without moving horizontally. The second approach is to suspend a payload with cables. In [5], an adaptive controller is presented to avoid swing excitation of a payload. In [6]–[8], specific attitude and position of a payload is achieved using cables connected to one or three quadrotors. However, this approach has a drawback that the movement of the payload cannot be always regulated directly because manipulation is achieved using a cable which cannot always drive the motion of the payload as desired.

To overcome these limitations, a third approach is developed in which an aerial vehicle is equipped with a robotic manipulator that can actively interact with the environment. For example, in [9], a test bed including two 4-DOF robot arms and a crane emulating an aerial robot is proposed. By combining the mobility of the aerial vehicle with the versatility of a robotic manipulator, the utility of mobile manipulation can be maximized. When employing the robotic manipulator, the dynamics of the robotic manipulator are highly coupled with that of the aerial vehicle, which should be carefully considered in the controller design. Also, an aerial robot needs to tolerate the reaction forces from the interactions with the object or external environment. These reaction forces may affect the stability of an aerial vehicle significantly. Very few reports that exist in the literature investigate the combination of aerial vehicle with the robotic manipulator. Kinematic and dynamic models of the quadrotor combined with arbitrary multi-DOF robot arm are derived using the Euler–Lagrangian formalism in [10]. Based on that, simulation results using the Cartesian impedance control for the combined system with 3-DOF robotic arm is presented in [11]. In addition, the effects of manipulators, two 4-DOF arms, on the quadrotor are simulated based on the dynamic model which considers a quadrotor and robotic arms separately, treating the arms as the disturbance to the quadrotor control loop. In [12], a quadrotor with lightweight manipulators, three 2-DOF arms, are tested, although the movement of the manipulators is not explicitly considered during the design of the proportional–integral–derivative controller. In [13], an aerial manipulation using a quadrotor with a 2-DOF robotic arm is presented but with certain topology that disable the system from making arbitrary position and orientation of the end-effector. In this system, the axes of the manipulator joints are parallel to each other and parallel to one in-plane axis of the quadrotor. Thus, the system cannot achieve orientation around the second in-plane axis of the quadrotor without moving horizontally.

From the above discussion, the systems that use a gripper suffer from the limited allowable DOF of the end-effector. The other systems have a manipulator with either two DOF but in certain topology that disables the end-effector to track arbitrary 6-DOF trajectory, or more than two DOF which decreases greatly the possible payload carried by the system.

In [14], [15], Khalifa *et al.* propose a new aerial manipulation system that consists of two-link manipulator, with two revolute joints whose axes are perpendicular to each other and the axis of the first joint is parallel to one in-plane axis of the quadrotor. Thus, the end-effector is able to reach arbitrary position and orientation without moving horizontally. However, the proof that this system can perform any desired trajectory in the task space has not been achieved yet due to the resulted complications in the inverse kinematics and control. This system is similar to a serial manipulator with eight joints, two of them are passive.

This system opens new application area for robotics. Such applications are inspection, maintenance, firefighting, service robot in crowded cities to deliver light stuff such as post mails or quick meals, rescue operation, surveillance, demining, performing tasks in dangerous places, or transportation in remote places.

The main contributions of this paper are as follows.

1) New quadrotor-based aerial manipulator, which utilizes a two-link robotic arm with unique topology, such that the end-effector can track a desired 6-DOF trajectory, is designed. This system is nonredundant and use minimum possible number of actuators and links such that the payload carried by the system can be maximized and consequently, the practical use can be enhanced.
2) Novel inverse kinematics analysis, which is based on complex set of nonlinear differential and algebraic equations, is presented and utilized to prove the end-effector ability to track an arbitrary 6-DOF trajectory that lays within the capability of the used actuators.
3) Design of a robust motion control scheme, with rigorous stability analysis, is carried out to track the desired 6-DOF trajectory.

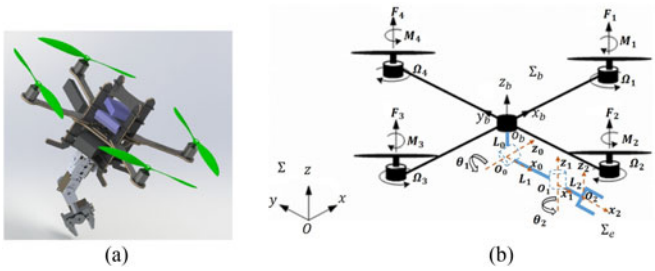

Fig. 1. Model of the proposed aerial manipulator. (a) Three-dimensional CAD model. (b) Schematic with relevant frames.

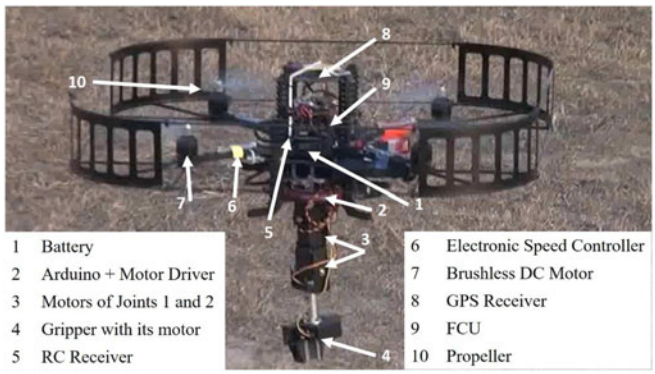

Fig. 2. Prototype of the proposed aerial manipulator.

II. Description and Design of the Proposed System

Three-dimensional (3-D) computer-aided design (CAD) model of the proposed system is shown in Fig. 1(a). The system consists mainly of two parts; the quadrotor and the manipulator. Fig. 1(b) presents a sketch of the proposed system with the relevant frames which indicates the unique topology that permits the end-effector to achieve arbitrary pose. The frames are assumed to satisfy the Denavit–Hartenberg convention. The manipulator has two revolute joints. The axis of the first revolute joint (z_0), that is fixed to the quadrotor, is parallel to the body x-axis of the quadrotor [see Fig. 1(b)]. The axis of the second joint (z_1) is perpendicular to the axis of the first joint and will be parallel to the body y-axis of the quadrotor at home (extended) configuration. Thus, the pitching and rolling rotation of the end-effector is now possible independently from the horizontal motion of the quadrotor. Hence, with this new system, the capability of manipulating objects with arbitrary location and orientation is achieved. By this nonredundant system, the end-effector can achieve 6-DOF motion with minimum number of actuators/links which is an important factor in flight. The proposed system is distinguished from all other previous systems in the literature by having maximum mobility with minimum weight. The resulted complexity of the inverse kinematics and control are handled later to prove the capability of the end-effector to track the reference 6-DOF trajectory.

The prototype of the proposed system is presented in Fig. 2. The quadrotor is selected such that it can carry an additional weight equals 500 g (larger than the total arm weight and the maximum payload). Asctec pelican quadrotor [16] is used as the quadrotor platform. It has a flight control unit (FCU) as well as a modular carbon fiber structure which enables us to easily mount different components like computer boards, position sensors, and the robotic arm with its electronics. The FCU has an inertial measurement unit (IMU) as well as two 32-Bit, 60 MHz ARM-7 microcontrollers. One of these microcontrollers, the low-level processor (LLP), is responsible for the hardware management and IMU sensor data fusion. The other microcontroller, high-level processor, is dedicated for custom code such as a new control algorithm. The IMU provides the accelerations and the angular velocities. It contains also a magnetic compass. It has a global positioning system receiver. A 11.1 V Li-Po battery is used as a power supply to the whole system. The angular position and angular velocity are available from the FCU via the IMU data fusion algorithm implemented in the LLP. The linear position and linear velocity can be obtained via data fusion of an on-board IMU and either monocular vision system [17], [18] or range finders (laser or ultrasonic) [19].

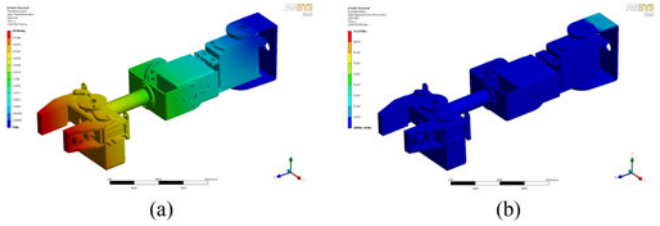

Fig. 3. Manipulator's structure analysis. (a) Deflection analysis. (b) Stress analysis.

A lightweight manipulator that can carry a payload of 200 g and has a maximum reach of 22 cm is designed. The arm components are selected, purchased, and assembled. Its weight is 200 g. The arm components are as follows. Three dc motors; HS-422 (Max torque = 0.4 N·m) for the gripper, HS-5485HB (Max torque = 0.7 N·m) for joint 1, and HS-422 (Max torque = 0.4 N·m) for joint 2. Motor's Driver (SSC) is used as an interface between the main control unit and the motors. Wireless PS2 R/C is used to send commands to manipulator's motors remotely. The manipulator structure accessories are aluminum tubing—1.50 in diameter, aluminum multipurpose servo bracket, Aluminum tubing connector hub, and aluminum long "C' servo bracket with ball bearings [20]. An Arduino board (Mega 2560) is utilized as an interface between the low-level peripherals (such as ultrasonic sensor, PS2 wireless receiver, and motor driver), and the on-board computer.

The safety of this design, with respect to the strength and rigidity, is checked through finite element analysis using ANSYS software (see Fig. 3). A 250 g force is applied at the gripper end, while the arm end (i.e., point at which the arm is connected to the body center of the quadrotor) is fixed. From these figures, the maximum deflection is about 0.6 mm which is smaller than the allowable value which equals 1 mm. In addition, the maximum stress of the structure is 113 MPa which is smaller than the yield strength of aluminum alloy which is 270 MPa. Also, the bearings and gripper are selected to sustain the loads. Therefore,

this design is safe. A prototype of the proposed system is built and its design is verified through flight test.[1]

III. Forward Kinematics

In this section, position and velocity kinematics analysis are presented. Let Σ_b, O_b- x_b y_b z_b denote the vehicle body-fixed reference frame with origin at the quadrotor center of mass [see Fig. 1(b)]. Its position with respect to the world-fixed inertial reference frame Σ, O- x y z is given by the (3×1) vector $p_b = [x\ y\ z]^T$, while its orientation is given by the rotation matrix R_b

$$R_b = \begin{bmatrix} C_\psi C_\theta & S_\phi S_\theta C_\psi - S_\psi C_\phi & S_\psi S_\phi + C_\psi S_\theta C_\phi \\ S_\psi C_\theta & C_\psi C_\phi + S_\psi S_\theta S_\phi & S_\psi S_\theta C_\phi - C_\psi S_\phi \\ -S_\theta & C_\theta S_\phi & C_\theta C_\phi \end{bmatrix} \tag{1}$$

where $\Phi_b = [\psi\ \theta\ \phi]^T$ is the triple ZYX yaw-pitch-roll angles. Note that $C_.$ and $S_.$ are short notations for $\cos(.)$ and $\sin(.)$, respectively. Let us consider the frame Σ_e, O_2- x_2 y_2 z_2 attached to the end-effector of the manipulator [see Fig. 1(b)].

Thus, the position of Σ_e with respect to Σ is given by

$$p_e = p_b + R_b p^b_{eb} \tag{2}$$

where the vector p^b_{eb} describes the position of Σ_e with respect to Σ_b expressed in Σ_b. The orientation of Σ_e can be defined by the rotation matrix

$$R_e = R_b R^b_e \tag{3}$$

where R^b_e describes the orientation of Σ_e w.r.t Σ_b. The forward kinematics problem consists of determining the operational coordinates $\chi_e = [x_e\ y_e\ z_e\ \psi_e\ \theta_e\ \phi_e]^T$, as a function of the vehicle/joint space coordinates $q = [x\ y\ z\ \psi\ \theta\ \phi\ \theta_1\ \theta_2]^T$. For solving the forward kinematics, the inputs are eight variables, q, and the output are six variables, χ_e, obtained from six algebraic equations. The end-effector position can be found from (2). Euler angles of the end-effector Φ_e can be computed from the rotation matrix of R_e, from (3).

In the rest of this section, the velocity kinematics analysis is discussed. The linear velocity $\dot{p}_e$ of Σ_e in the world-fixed frame is obtained by the differentiation of (2) as

$$\dot{p}_e = \dot{p}_b - \text{Skew}(R_b p^b_{eb})\omega_b + R_b \dot{p}^b_{eb}, \tag{4}$$

where Skew$(.)$ is the (3×3) skew-symmetric matrix operator, while ω_b is the angular velocity of the quadrotor expressed in Σ. The angular velocity ω_e of Σ_e is expressed as

$$\omega_e = \omega_b + R_b \omega^b_{eb} \tag{5}$$

where ω^b_{eb} is the angular velocity of the end-effector relative to Σ_b and is expressed in Σ_b.

Let $\Theta = [\theta_1\ \theta_2]^T$ be the (2×1) vector of joint angles of the manipulator. The (6×1) vector of the generalized velocity of the end-effector with respect to Σ_b, $v^b_{eb} = [\dot{p}^{bT}_{eb}\ \omega^{bT}_{eb}]^T$, can be expressed in terms of the joint velocities $\dot{\Theta}$ via the manipulator Jacobian, J^b_{eb}, such that

$$v^b_{eb} = J^b_{eb}\dot{\Theta}. \tag{6}$$

From (4) and (5), the generalized end-effector velocity, $v_e = [\dot{p}^T_e\ \omega^T_e]^T$, can be expressed as

$$v_e = J_b v_b + J_{eb}\dot{\Theta} \tag{7}$$

where $v_b = [\dot{p}^T_b\ \ \omega^T_b]^T$, $J_b = \begin{bmatrix} I_3 & -\text{Skew}(R_b p^b_{eb}) \\ O_3 & I_3 \end{bmatrix}$, $J_{eb} = \begin{bmatrix} R_b & O_3 \\ O_3 & R_b \end{bmatrix} J^b_{eb}$ where I_m and O_m denote $(m\times m)$ identity and $(m\times m)$ null matrices, respectively. If the attitude of the vehicle is expressed in terms of yaw-pitch-roll angles, then (7) will be

$$v_e = J_b Q_b \chi_b + J_{eb}\dot{\Theta} \tag{8}$$

with $\chi_b = \begin{bmatrix} p_b \\ \Phi_b \end{bmatrix}$, $Q_b = \begin{bmatrix} I_3 & O_3 \\ O_3 & T_b \end{bmatrix}$, where T_b describes the transformation matrix between the angular velocity ω_b and the time derivative of Euler angles $\dot{\Phi}_b$, and it is given as

$$T_b(\Phi_b) = \begin{bmatrix} 0 & -S_\psi & C_\psi C_\theta \\ 0 & C_\psi & S_\psi C_\theta \\ 1 & 0 & -S_\theta \end{bmatrix}. \tag{9}$$

Since the vehicle is an underactuated system, i.e., only four independent control inputs are available for the 6-DOF system, the position and the yaw angle are usually the controlled variables. Hence, it is worth to define $\zeta = [x\ y\ z\ \psi\ \theta_1\ \theta_2]^T$ as the controlled variables and $\sigma_b = [\theta\ \phi]^T$ as the intermediate variables.

IV. Dynamic Model

The equations of motion of the proposed robot have been derived by us in details in [14]. Applying the Newton Euler algorithm to the manipulator, one can get the equations of motion of the manipulator as well as the interaction forces and moments between the manipulator and the quadrotor.

For the system structure, we assume the following.

Assumption 1: The quadrotor body is rigid and symmetric. The manipulator links are rigid.

The equations of motion of the manipulator are

$$M_1(q)\ddot{\theta}_1 + N_1(q,\dot{q},\ddot{\chi}_b) = \tau_{m_1}, \tag{10}$$

$$M_2(q)\ddot{\theta}_2 + N_2(q,\dot{q},\ddot{\chi}_b) = \tau_{m_2} \tag{11}$$

where τ_{m_1} and τ_{m_2} are the manipulator actuators' torques. $M_1(q)$, $M_2(q)$, $N_1(q,\dot{q},\ddot{\chi}_b)$, and $N_2(q,\dot{q},\ddot{\chi}_b)$ are nonlinear terms and they are functions of the system states $(q,\ \dot{q})$ and accelerations $(\ddot{\chi}_b)$.

The Newton Euler method are used to find the equations of motion of the quadrotor after adding the forces/moments from the manipulator. They are given by the following equations:

$$m\ddot{x} = T(C_\psi S_\theta C_\phi + S_\psi S_\phi) + F_{m,q_x} \tag{12}$$

$$m\ddot{y} = T(S_\psi S_\theta C_\phi - C_\psi S_\phi) + F_{m,q_y} \tag{13}$$

$$m\ddot{z}p = -mg + TC_\theta C_\phi + F_{m,q_z} \tag{14}$$

$$I_x\ddot{\phi} = \dot{\theta}\dot{\phi}(I_y - I_z) - I_r\dot{\theta}\overline{\Omega} + T_{a_1} + M^b_{m,q_\phi} \tag{15}$$

[1] https://www.dropbox.com/s/g9psmcbici3mphk/Prototype_Test.avi?dl=0

$$I_y\ddot{\theta} = \dot{\psi}\dot{\phi}(I_z - I_x) + I_r\dot{\phi}\overline{\Omega} + T_{a_2} + M^b_{m,q_\theta} \tag{16}$$

$$I_z\ddot{\psi} = \dot{\theta}\dot{\phi}(I_x - I_y) + T_{a_3} + M^b_{m,q_\psi} \tag{17}$$

where F_{m,q_x}, F_{m,q_y}, and F_{m,q_z} are the interaction forces from the manipulator to the quadrotor in x, y, and z directions expressed in the inertial frame and M^b_{m,q_ϕ}, M^b_{m,q_θ}, and M^b_{m,q_ψ} are the interaction moments from the manipulator to the quadrotor around x_b, y_b, and z_b directions.

The variables in (12)–(17) are defined as follows: m is the mass of the quadrotor. Each rotor j has angular velocity Ω_j and it produces thrust force F_j and drag moment M_j which are given by

$$F_j = K_{f_j}\Omega_j^2, \quad M_j = K_{m_j}\Omega_j^2 \tag{18}$$

where K_{f_j} and K_{m_j} are the thrust and drag coefficients, respectively.

T is the total thrust applied to the quadrotor from all four rotors. T_{a_1}, T_{a_2}, and T_{a_3} are the three input moments about the three body axes, x_b, y_b, and z_b, respectively. d is the distance between the quadrotor center of mass and rotor rotational axis. $\overline{\Omega}$ is given by

$$\overline{\Omega} = \Omega_1 - \Omega_2 + \Omega_3 - \Omega_4. \tag{19}$$

I_r is the rotor inertia. I_f is the inertia matrix of the vehicle around its body-frame assuming that the vehicle is symmetric about x_b-, y_b-, and z_b-axis.

The dynamical model of the quadrotor-manipulator system can be written as follows:

$$M(q)\ddot{q} + C(q,\dot{q})\dot{q} + G(q) + d_{\text{ex}} = Bu \tag{20}$$

where $M \in R^{8\times 8}$ represents the symmetric and positive definite inertia matrix of the combined system, $C \in R^{8\times 8}$ is the matrix of Coriolis and centrifugal terms, $G \in R^8$ is the vector of gravity terms, $d_{\text{ex}} \in R^8$ is vector of the external disturbances, $u = [F_1\ F_2\ F_3\ F_4\ \tau_{m_1}\ \tau_{m_2}]^T \in R^6$ is vector of the actuator inputs, and $B = H(q)\ N(K_{f_j}, K_{m_j}, d)$ is the input matrix which is used to generate the body forces and moments from the actuator inputs. The control matrix N is given by

$$N = \begin{bmatrix} 0 & 0 & 0 & 0 & 0 & 0 \\ 0 & 0 & 0 & 0 & 0 & 0 \\ 1 & 1 & 1 & 1 & 0 & 0 \\ \gamma_1 & -\gamma_2 & \gamma_3 & -\gamma_4 & 0 & 0 \\ -d & 0 & d & 0 & 0 & 0 \\ 0 & -d & 0 & d & 0 & 0 \\ 0 & 0 & 0 & 0 & 1 & 0 \\ 0 & 0 & 0 & 0 & 0 & 1 \end{bmatrix} \tag{21}$$

where $\gamma_j = K_{m_j}/K_{f_j}$, and $H \in R^{8\times 8}$ is the matrix that transforms body input forces to be expressed in Σ and is given by

$$H = \begin{bmatrix} R_b & O_3 & O_2 \\ O_3 & T_b^T R_b & O_2 \\ O_{2\times 3} & O_{2\times 3} & I_2 \end{bmatrix}. \tag{22}$$

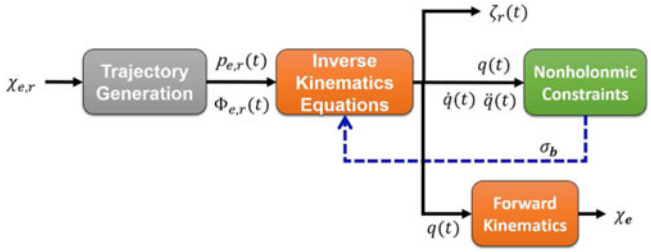

Fig. 4. Verification of the inverse kinematic algorithm: Block diagram.

From the equations of the translation dynamics part of (12)–(14), one can extract the expressions of the second-order nonholonomic constraints as

$$\sin(\phi) - \frac{\ddot{x}_f S_\psi - \ddot{y}_f C_\psi}{\sqrt{\ddot{x}_f^2 + \ddot{y}_f^2 + \ddot{z}_f^2}} = 0 \tag{23}$$

$$\tan(\theta) - \frac{\ddot{x}_f C_\psi + \ddot{y}_f S_\psi}{\ddot{z}_f} = 0 \tag{24}$$

where $\ddot{x}_f = \ddot{x} - \frac{F_{m,q_x}}{m}$, $\ddot{y}_f = \ddot{y} - \frac{F_{m,q_y}}{m}$, and $\ddot{z}_f = \ddot{z} + g - \frac{F_{m,q_z}}{m}$.

It is to be noted that the force terms in the above equations are also function of the system states and their derivatives. Equations (23) and (24) can be solved for the desired trajectories of ϕ and θ through substituting by the desired trajectories of the other variables. These nonholonomic constraints will be utilized later to solve the inverse kinematics problem.

V. Inverse Kinematics

A task for the quadrotor manipulation system is usually specified in terms of a desired trajectory for the end-effector position, $p_{e,r}(t)$, and orientation, $\Phi_{e,r}(t)$. In this section, six algebraic kinematic equations relating χ_e with q are derived.

However, to find the eight variables of q from the given six variables of χ_e, we need additional two equations. These two equations are the nonholonomic constraints (23) and (24) which are differential equations. We solve these eight equation symbolically and reduce them to two differential equations in σ_b. It is found that the exact solution of them has very high computation cost which prevents its practical implementation.

For the desired task space trajectories, we assume the following.

Assumption 2: The desired trajectories for the end-effector are bounded.

Thus, we propose an algorithm to get an approximate solution to these eight algebraic/differential equations, see Fig. 4, as follows.

1) Specify the desired 6-DOF trajectory in the task space, $\chi_{e,r}(t)$.
2) Put $i = 1$, $t_1 = 0$, and $\Delta t =$ very small positive number (1 ms).
3) Put $\sigma_b(t_0) = \dot{\sigma}_b(t_0) = \ddot{\sigma}_b(t_0) = [0\ 0]^T$.
4) At time t_i, obtain the values of $\chi_{e,r}(t_i)$ and put $\sigma_b(t_i) = \sigma_b(t_{i-1})$, $\dot{\sigma}_b(t_i) = \dot{\sigma}_b(t_{i-1})$, and $\ddot{\sigma}_b(t_i) = \ddot{\sigma}_b(t_{i-1})$.

5) Use the six inverse kinematics algebraic equations and get the unknowns $\zeta_r(t_i)$, $\dot{\zeta}_r(t_i)$, $\ddot{\zeta}_r(t_i)$ which with $\sigma_b(t_i)$, $\dot{\sigma}_b(t_i)$, and $\ddot{\sigma}_b(t_i)$ constitute $q(t_i)$, $\dot{q}(t_i)$, and $\ddot{q}(t_i)$.
6) In the equations of the nonholonomic constraints, we separate sin (ϕ) and tan (θ) in one side (left side) and the other terms in the other side (right side).
7) We substitute by $q(t_i)$, $\dot{q}(t_i)$, $\ddot{q}(t_i)$ values in the right-hand side of the nonholonomic constraints obtained from step 6, and obtain the new $\sigma_b(t_i)$ from left-hand side and by numerical differentiation, one can get the new $\dot{\sigma}_b(t_i)$ and $\ddot{\sigma}_b(t_i)$.
8) Put $i = i + 1$, $t_i = t_{i-1} + \Delta t$, and repeat steps 4 to 8 to obtain the reference trajectories of the controlled variables $\zeta_r(t_i)$.

The validation of this algorithm will be checked at the end of this section. The six algebraic inverse kinematic equations are derived next.

Define the general form for the rotation matrix R_e as a function of end-effector variables χ_e, as

$$R_e = \begin{bmatrix} r_{11} & r_{12} & r_{13} \\ r_{21} & r_{22} & r_{23} \\ r_{31} & r_{32} & r_{33} \end{bmatrix}. \tag{25}$$

Equating (3) and (25), an expression for the elements of R_e, r_{ij}; $i, j = 1, 2, 3$, can be found. According to the structure of R_e from (3), the inverse orientation is carried out first followed by inverse position. The inverse orientation has three cases based on the value of θ_1 which can be calculated from the element r_{33} as

$$C_\phi C_\theta C_{\theta_1} - S_\phi C_\theta S_{\theta_1} = r_{33}. \tag{26}$$

By rearranging (26) and solving the resulting equation for θ_1, then

$$\theta_1 = 2\,\mathrm{atan2}(-2b_1 \pm \sqrt{(2b_1)^2 - 4(-a_1 - r_{33})(a_1 - r_{33})}, \\ 2(-a_1 - r_{33})) \tag{27}$$

where $a_1 = C_\phi C_\theta$ and $b_1 = -S_\phi C_\theta$.

The three cases are derived as follows.

Case 1: $\theta_1 \neq 0$ and $\theta_1 \neq \pi$

Inspecting r_{13} and r_{23}, one can find the value of ψ as

$$r_{13} = a_2 S_\psi + b_2 C_\psi, \tag{28}$$

$$r_{23} = c_2 S_\psi + d_2 C_\psi \tag{29}$$

where $a_2 = C_\phi S_{\theta_1} + S_\phi C_{\theta_1}$, $b_2 = C_\phi S_\theta C_{\theta_1} - S_\phi S_\theta S_{\theta_1}$, $c_2 = b_2$, and $d_2 = -a_2$.

Solving (28) and (29) will give

$$S_\psi = \frac{r_{23} b_2 - r_{13} d_2}{-d_2 a_2 + b_2 c_2}, \tag{30}$$

$$C_\psi = \frac{r_{23} a_2 - r_{13} c_2}{d_2 a_2 - b_2 c_2}, \tag{31}$$

$$\psi = \mathrm{atan2}(S_\psi, C_\psi). \tag{32}$$

By inspecting r_{32} and r_{31}, θ_2 can be found as

$$r_{32} = a_3 S_{\theta_2} + b_3 C_{\theta_2}, \tag{33}$$

$$r_{31} = c_3 S_{\theta_2} + d_3 C_{\theta_2} \tag{34}$$

where $a_3 = C_\phi C_\theta S_{\theta_1} + C_\theta S_\phi C_{\theta_1}$, $b_3 = -S_\theta$, $c_3 = b_3$, and $d_3 = -a_3$.

Solving (33) and (34), then

$$S_{\theta_2} = \frac{r_{31} b_3 - r_{32} d_3}{-d_3 a_3 + b_3 c_3}, \tag{35}$$

$$C_{\theta_2} = \frac{r_{31} a_3 - r_{32} c_3}{d_3 a_3 - b_3 c_3}, \tag{36}$$

$$\theta_2 = \mathrm{atan2}(S_{\theta_2}, C_{\theta_2}). \tag{37}$$

Case 2: $\theta_1 = 0$

If $\theta_1 = 0$, then the sum $\theta_2 + \psi$ can be determined. One can assume any value for ψ and get θ_2. Therefore, there are infinity of solutions. By putting $\psi = 0$, the value of θ_2 can be determined as follows.

Inspecting r_{11} and r_{12}, θ_2 can be found as

$$r_{11} = a_4 S_{\theta_2} + b_4 C_{\theta_2}, \tag{38}$$

$$r_{12} = c_4 S_{\theta_2} + d_4 C_{\theta_2} \tag{39}$$

where $a_4 = C_\theta$, $b_4 = -S_\phi S_\theta$, $c_4 = -b_4$, and $d_4 = a_4$.

Solving (38) and (39), then

$$S_{\theta_2} = \frac{r_{12} b_4 - r_{11} d_4}{-d_4 a_4 + b_4 c_4}, \tag{40}$$

$$C_{\theta_2} = \frac{r_{12} a_4 - r_{11} c_4}{d_4 a_4 - b_4 c_4}, \tag{41}$$

$$\theta_2 = \mathrm{atan2}(S_{\theta_2}, C_{\theta_2}). \tag{42}$$

Case 3: $\theta_1 = \pi$

Since $S_{\theta_1} = 0$, this is similar to case 2. However, $\theta_2 - \psi$ can be determined and by choosing $\psi = 0$, an expression for θ_2 can be determined as follows.

Inspecting r_{11} and r_{12}, θ_2 can be found as

$$r_{11} = a_5 S_{\theta_2} + b_5 C_{\theta_2}, \tag{43}$$

$$r_{12} = c_5 S_{\theta_2} + d_5 C_{\theta_2} \tag{44}$$

where $a_5 = a_4$, $b_5 = -b_4$, $c_5 = -b_5$, and $d_5 = a_5$.

Solving (43) and (44), then

$$S_{\theta_2} = \frac{r_{12} b_5 - r_{11} d_5}{-d_5 a_5 + b_5 c_5}, \tag{45}$$

$$C_{\theta_2} = \frac{r_{12} a_5 - r_{11} c_5}{d_5 a_5 - b_5 c_5}, \tag{46}$$

$$\theta_2 = \mathrm{atan2}(S_{\theta_2}, C_{\theta_2}). \tag{47}$$

As shown above, there are four possible solutions for the rotational inverse kinematics problem provided that we put $\psi = 0$ in cases 2 and 3. When we start applying the above-described algorithm in real time, we select the solution of θ_1 which coincides with the given configuration of the quadrotor manipulation system. After that, we continue with the one of the four solutions which produces this θ_1.

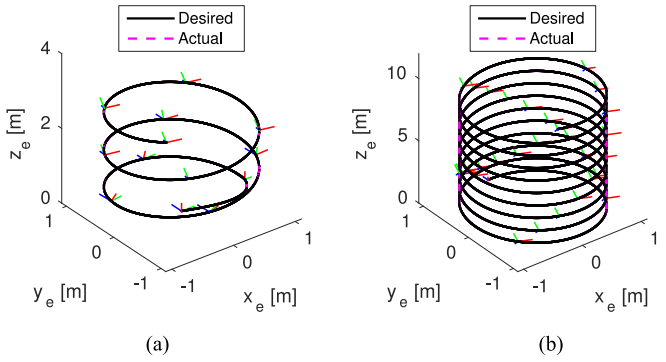

Fig. 5. Verification of the inverse kinematic algorithm: End-effector 3-D trajectory. (a) Slower trajectory. (b) Faster trajectory.

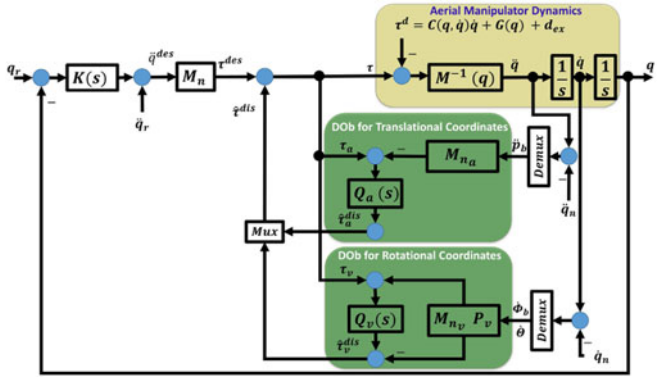

Fig. 6. Block diagram of DOb-based controller.

Finally, the inverse position is determined from (2) as

$$p_b = p_e - R_b p_{eb}^b. \tag{48}$$

To validate the proposed approximate solution of the inverse kinematics, the desired task space trajectories are chosen to make a circular helix in position and quintic polynomial [21] for the orientation.

After obtaining the joint space variables from the proposed algorithm, as shown in Fig. 4, we apply the forward kinematics to find the actual task space trajectory.

The comparison between the actual and desired task space trajectories is shown in Fig. 5(a) from which one can recognize that the actual and desired trajectories coincide. In Fig. 5(b), another case study is investigated to show the capability of the proposed algorithm to deal with higher speed desired trajectories. In this study, the desired trajectories are chosen to be faster than that in Fig. 5(a) by ten times. These figures show that the actual and desired trajectories coincide under both slower or faster trajectories, which ensures the validity of the proposed inverse kinematic algorithm, and proves that the proposed system has the ability to track arbitrary 6-DOF task space trajectory. With this result in mind, we propose a control algorithm in the next section to track the desired 6-DOF trajectories in the task space.

VI. Control Design

A. Control Objectives

We target the design of the controller output, τ, in order to satisfy the following objectives.

1) *Control Objective 1 (Robust Stability):* The considered robotic system is stable and robust in the presence of the external disturbances and noises.
2) *Control Objective 2:* Minimizing the error of the 6-DOF task space trajectory tracking.

To achieve these control objectives, we utilize a control technique based on both the DOb method and the above inverse kinematics analysis.

B. DOb-Based Controller

DOb-based controller is one of the most popular methods in the field of robust motion control due to its simplicity and computational efficiency. Kim and Chung [22], and Li *et al.* [23] present the principles of DOb-based control system. In DOb-based robust motion control systems, internal and external disturbances are observed by DOb, and the robustness is simply achieved by feeding-back the estimated disturbances in an inner loop. Another controller is designed in an outer loop so that the performance goals are achieved without considering internal and external disturbances. In [24]–[26], DOb-based control technique has been applied to robotic systems and showed efficient performance.

A block diagram of the DOb controller is shown in Fig. 6 (the plant dynamics are highlighted by yellow box, while the dob loops are highlighted by green box) for robotic system which will be utilized later to design robust control for the proposed system. It is well known that the linear accelerations and angular rates of the vehicle can be measured directly from IMU. In addition, the angular velocities of the manipulator joints can be measured via an encoder. Therefore, two different DOb loops are used. One is based on the measured acceleration, while the other is based on the measured velocity.

In Fig. 6, $M_n = \left[\begin{smallmatrix} M_{n_a} & O_{3\times5} \\ O_{5\times3} & M_{n_v} \end{smallmatrix}\right] \in R^{8\times8}$ is the system nominal inertia matrix with $M_{n_a} \in R^{3\times3}$ represents the nominal inertia for the translational coordinates p_b, while $M_{n_v} \in R^{5\times5}$ represents the nominal inertia for the rotational coordinates, Φ_b and Θ. τ^{des} is the robot desired input. $\tau = [\tau_a^T \ \tau_v^T]^T$ is the robot generalized input. $Q(s) = \left[\begin{smallmatrix} Q_a & O_{3\times5} \\ O_{5\times3} & Q_v \end{smallmatrix}\right] \in R^{8\times8}$ is the matrix of the low-pass filter of DOb, $Q_a(s) = \text{diag}([\frac{g_1}{s+g_1} \ \ldots \ \frac{g_3}{s+g_3}])$, and $Q_v(s) = \text{diag}([\frac{g_4}{s+g_4} \ \ldots \ \frac{g_8}{s+g_8}])$. $P = \left[\begin{smallmatrix} P_a & O_{3\times5} \\ O_{5\times3} & P_v \end{smallmatrix}\right]$ with $P_a = \text{diag}([g_1 \ g_2 \ g_3])$ for the translational coordinates and $P_v = \text{diag}([g_4 \ \ldots \ g_i \ \ldots \ g_8])$ for the rotational coordinates, where g_i is the bandwidth of the ith variable of q. τ^{dis} represents the system disturbances including the Coriolis, centrifugal and gravitational terms in addition to external disturbance. $\hat{\tau}^{\text{dis}} = [\hat{\tau}_a^{\text{dis}^T} \ \hat{\tau}_v^{\text{dis}^T}]^T$ (collected by the block called Mux, like multiplexer symbol in MATLAB) represents the system estimated disturbances. $\dot{q}_n$ and $\ddot{q}_n$ represent the measurement noise of the velocity and acceleration, respectively. The block named "Demux" is a demultiplexer which is used to select some signals from bus of signals. It is used, for example, to select the linear accelerations $\ddot{p}_b$, from the accelerations vector of the whole system, $\ddot{q}$.

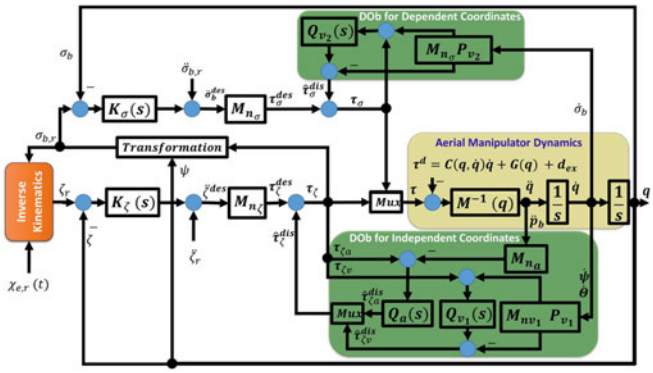

Fig. 7. Detailed block diagram of the control system.

The system disturbance τ^{dis} can be assumed as

$$\tau^{\text{dis}} = (M(q) - M_n)\ddot{q} + \tau^d,$$
$$\tau^d = C(q,\dot{q})\dot{q} + G(q) + d_{\text{ex}}. \tag{49}$$

The control input, τ, in Fig. 6 can be calculated as

$$\tau = M_n \ddot{q}^{\text{des}} + \hat{\tau}^{\text{dis}} \tag{50}$$

where

$$\hat{\tau}^{\text{dis}} = Q(\tau - M_n \ddot{q}) \tag{51}$$

and $\ddot{q}^{\text{des}}$ is the output of the outer loop controller $K(s)$, and it is given as

$$\ddot{q}^{\text{des}} = \ddot{q}_r + K_P(q_r - q) + K_D(\dot{q}_r - \dot{q}) \tag{52}$$

where K_P and $K_D \in R^{8\times 8}$ are the proportional and derivative gains of the PD controller, respectively. q_r, $\dot{q}_r$, and $\ddot{q}_r$ are the references for linear/angular positions, velocities, and accelerations, respectively.

Thus, the control input, τ, can be calculated from (49)–(51) as

$$\tau = M_n \ddot{q}^{\text{des}} + K_v e_v \tag{53}$$

where $K_v = PM_n = k_v I_8$ with k_v is a positive constant, and $e_v = \dot{q}^{\text{des}} - \dot{q}$ with $\ddot{q}^{\text{des}}$ is the output from the outer loop controller.

Fig. 7 presents a block diagram of the proposed motion control system based on the inverse kinematics analysis and on quadrotor/joint space-based control. The desired trajectories for the end-effector's position and orientation $\chi_{e,r}(t)$ are fed to the inverse kinematics algorithm together with $\sigma_{b,r}(t)$ from a simplified version of the nonholonomic constraints (54) such that the desired vehicle/joint space trajectories $\zeta_r(t)$ are obtained. After that, the controller block receives the desired trajectories and the feedback signals from the system and provides the control signal, $\tau = Bu$.

Since the quadrotor position, manipulator joints angles, and the yaw angle are usually the controlled variables (i.e., independent coordinates, ζ), while pitch and roll angles are used as intermediate control inputs (i.e., dependent coordinates, σ_b) for horizontal positions control, the proposed control system consists of two DOb-based controllers; one for ζ (with $K_\zeta(s)$, M_{n_a}, M_{nv_1}, P_{v_1}, Q_{v_1}, and Q_a) and the other for σ_b (with $K_\sigma(s)$, M_{n_σ}, P_{v_2}, Q_{v_2}). The subscript v_1 refers to the rotational motion in the independent coordinates which are ψ, θ_1, and θ_2, while the subscript v_2 refers to the rotational motion in the dependent coordinates which are $\sigma_b = [\theta\ \phi]^T$.

The desired independent quadrotor/joint space trajectories generated from the inverse kinematics algorithm ζ_r are fed to the PD controller $K_\zeta(s)$ that will produce the desired acceleration for the independent coordinates $\ddot{\zeta}^{\text{des}}$. This desired acceleration $\ddot{\zeta}^{\text{des}}$ is converted to a desired torque τ_ζ^{des} via multiplication by the nominal inertia matrix of the independent coordinates M_{n_ζ}. The desired torque is added to the estimated disturbances, $\hat{\tau}_\zeta^{\text{dis}} = [\hat{\tau}_{\zeta a}^{\text{dis}^T}\ \hat{\tau}_{\zeta v}^{\text{dis}^T}]^T$, from the DOb of the independent coordinates ζ, such that the required input torques in the independent coordinates τ_ζ are produced. Inside the lower DOb block there are two DObs. The first one is for the translation independent coordinates p_b. It is an acceleration-based DOb, with inputs as system linear accelerations and the input torques for the translational motion $\tau_{\zeta a} = \tau_\zeta(1:3)$. It uses the corresponding part of the low-pass filter Q_a and the corresponding part of the nominal inertia matrix M_{n_a}. This block produces the estimated disturbances for the translational motion $\hat{\tau}_{\zeta a}^{\text{dis}}$. The second DOb inside the lower DOb block is for the rotational independent coordinates, ψ, θ_1, and θ_2, and it is a velocity-based DOb, with inputs as rates of yaw and manipulator joints angles and the input torques for the independent rotational motion $\tau_{\zeta v} = \tau_\zeta(4:6)$. It uses the corresponding part of the low-pass filter Q_{v_1} the corresponding part of P_v, P_{v_1} and the corresponding part of the nominal inertia matrix M_{nv_1}. This block produces the estimated disturbances for the rotational motion $\hat{\tau}_{\zeta v}^{\text{dis}}$. After that, $\hat{\tau}_{\zeta a}^{\text{dis}}$ and $\hat{\tau}_{\zeta v}^{\text{dis}}$ are gathered to get the final estimated disturbances for the independent coordinates $\hat{\tau}_\zeta^{\text{dis}}$.

The desired values for the intermediate controller $\sigma_{b,r}$ are obtained from the output of independent coordinates' controller τ_ζ through the relation

$$\sigma_{b,r} = \frac{1}{\tau_\zeta(3)} \begin{bmatrix} C_\psi & S_\psi \\ S_\psi & -C_\psi \end{bmatrix} \begin{bmatrix} \tau_\zeta(1) \\ \tau_\zeta(2) \end{bmatrix} \tag{54}$$

which can be derived from (1) based on small angle approximation.

The desired value of the pitching and rolling $\sigma_{b,r}$ is then fed back to both the inverse kinematics algorithm and the outer loop controller for the dependent coordinates $K_\sigma(s)$. This controller produces the desired acceleration for the dependent coordinates $\ddot{\sigma}_b^{\text{des}}$ that is converted to desired torque τ_σ^{des} via the nominal inertia matrix of the rotational dependent coordinates M_{n_σ}. The desired torque is added to the estimated disturbances $\hat{\tau}_\sigma^{\text{dis}}$ from the DOb of the dependent coordinates σ_b, such that the required input torques for the dependent coordinates τ_σ are produced. The upper DOb block is a velocity-based DOb, with inputs as rate of σ_b and the input torque for the dependent rotational motion τ_σ. It uses the corresponding part of the low-pass filter Q_{v_2} the corresponding part of P_v, P_{v_2}, and the corresponding part of the nominal inertia matrix M_{n_σ}. This block produces the estimated disturbances for the dependent rotational motion $\hat{\tau}_\sigma^{\text{dis}}$.

After that, the output of the two controllers τ_ζ and τ_σ are mixed to generate the final control vector τ which is converted to the forces/torques applied to quadrotor/manipulator by

$$u = B_6^{-1} \begin{bmatrix} \tau_\zeta(3,4) \\ \tau_\sigma \\ \tau_\zeta(5,6) \end{bmatrix} \tag{55}$$

where $B_6 \in R^{6\times 6}$ is the part of B matrix and it is given by $B_6 = B(3:8, 1:6)$.

Theorem 1: Consider the control system shown in Fig. 7, and described in (20), (50), and (52) with *Assumptions* 1–2. Then, as long as the following conditions; $K_v > 0$, $K_P > 0$, and $K_D > 0$, are satisfied, the system is L_p input/output stable with respect to the pair (δ, e_v), and $e \in L_p$ and $\dot{e} \in L_p$ for all $p \in [1, \infty)$ such that

$$\|e_v\|_p \leq \frac{1}{\gamma} + \sqrt{\frac{2}{\lambda_{\min}}} \left(\frac{2}{p\gamma}\right)^{\frac{1}{p}} \sqrt{V(0, e_v(0))} \|\delta\|_p. \tag{56}$$

Proof: By substituting from the control law (52) and (53) into the system dynamics equation (20), one can get the following error dynamics:

$$M(q)\dot{e}_v + C(q,\dot{q})e_v + K_v e_v = \delta \tag{57}$$

and

$$\dot{e} + K_D e + K_P \int e\, dt = e_v \tag{58}$$

where

$$\delta = \Delta M(q)\ddot{q}^{\text{des}} + C(q,\dot{q})\dot{q}^{\text{des}} + G(q) + d_{\text{ex}} \tag{59}$$

and $\Delta M(q) = M(q) - M_n$.

Assume the following Lyapunov function:

$$V = \frac{1}{2} e_v^T M(q) e_v. \tag{60}$$

The time derivative of this function is

$$\dot{V} = e_v^T M(q)\dot{e}_v + \frac{1}{2} e_v^T \dot{M}(q) e_v. \tag{61}$$

Substituting from (57), then (61) becomes

$$\dot{V} = e_v^T \delta - e_v^T K_v e_v + \frac{1}{2} e_v^T (\dot{M}(q) - 2C(q,\dot{q})) e_v. \tag{62}$$

The dynamic equation of motion (20) posses several well-known properties [27].

Property 1:

$$\lambda_{\min}\|\nu\|^2 \leq \nu^T M(q)\nu \leq \lambda_{\max}\|\nu\|^2. \tag{63}$$

Property 2:

$$\nu^T (\dot{M}(q) - 2C(q,\dot{q}))\nu = 0 \tag{64}$$

where $\dot{M}(q) - 2C(q,\dot{q})$ is a skew-symmetric matrix, $\nu \in R^8$ represents a 8-D vector, and $\lambda_{\min}$ and $\lambda_{\max}$ are positive real constants.

Substituting from (64) into (62), then (62) will be

$$\dot{V} = e_v^T \delta - e_v^T K_v e_v. \tag{65}$$

From the robot dynamic property (63), one can find

$$\dot{V} \leq -\gamma V + \sqrt{\frac{2V}{\lambda_{\min}}} |\delta| \tag{66}$$

where $\gamma = \frac{2k_v}{\lambda_{\max}}$. From the analysis presented in [28] and [29], we complete the proof as the following. Dividing (66) by $V^{0.5} \neq 0$ will give

$$\frac{d}{dt}(V^{0.5}) + 0.5\gamma V^{0.5} \leq \sqrt{\frac{2}{\lambda_{\min}}} |\delta|. \tag{67}$$

By multiplying (67) by $e^{-0.5\gamma}$ and integrating, then we obtain

$$V^{0.5} \leq e^{-0.5\gamma t} V^{0.5}(0, e_v(0)) + V_c \tag{68}$$

with

$$V_c = \frac{1}{\sqrt{2\lambda_{\min}}} \int_0^t e^{-0.5\gamma(t-\iota)} |\delta(\iota)| d\iota. \tag{69}$$

We can rewrite V_c as

$$V_c = \frac{1}{\sqrt{2\lambda_{\min}}} (e^{-0.5\gamma t} * |\delta(t)|). \tag{70}$$

Taking the $\|.\|_p$, gives

$$\|V_c\|_p = \frac{1}{\sqrt{2\lambda_{\min}}} \|e\|^{-0.5\gamma t} * \|\delta(t)|_p. \tag{71}$$

From *Lemma* 3 in [29], then (71) is

$$\|V_c\|_p = \frac{1}{\sqrt{2\lambda_{\min}}} \|e\|^{-0.5}\gamma t_1 \|\delta(t)\|_p \tag{72}$$

but $\|e\|_1^{-0.5\gamma t} = 0.5\gamma$, so

$$\|V_c\|_p = 0.5\gamma \frac{1}{\sqrt{2\lambda_{\min}}} \|\delta(t)\|_p. \tag{73}$$

Thus, (68) is

$$\|V^{0.5}\|_p \leq \|e\|^{-0.5\gamma t} V^{0.5}(0, e_v(0))_p + 0.5\gamma \frac{1}{\sqrt{2\lambda_{\min}}} \|\delta(t)\|_p. \tag{74}$$

This expression (74) can be simplified to reach (56).

Lemma 1 ([30]): Let

$$e = H_{PD}(s) e_v \tag{75}$$

where $H_{PD}(s)$ is an strictly proper and exponentially stable transfer function. Then, $e_v \in L_p$ implies that $e \in L_p$ and $\dot{e} \in L_p$.

Form (58), the transfer function between e and e_v is proper exponentially stable as long as the parameters K_P and K_D are positive definite matrices. Thus, Lemma 1 implies that both e and $\dot{e} \in L_p$. ■

Remark 1: Equation (66) indicates that the convergence rate increases proportionally with K_v. However, we have to take into considerations the constraints on g_i due to the sampling time.

Remark 2: It is noted from the quadrotor dynamics [31] that the response of the intermediate σ controller must be faster than that of the position control loop. However, as stated in the above analysis, the convergence rate of errors dynamics (e_v and e) is directly proportional to the K_v, K_P, K_D. Therefore, we have

TABLE I
SYSTEM PARAMETERS

Par.	Value	Unit	Par.	Value	Unit
m	1	kg	L_2	85×10^{-3}	m
d	223.5×10^{-3}	m	m_0	30×10^{-3}	kg
I_x	13.215×10^{-3}	N·m.s^2	m_1	55×10^{-3}	kg
I_y	12.522×10^{-3}	N·m.s^2	m_2	112×10^{-3}	kg
I_z	23.527×10^{-3}	N·m.s^2	I_r	33.216×10^{-6}	N·m.s^2
L_0	30×10^{-3}	m	L_1	70×10^{-3}	m
K_{F_1}	1.667×10^{-5}	kg.m.rad^2	K_{F_2}	1.285×10^{-5}	kg.m.rad^2
K_{F_3}	1.711×10^{-5}	kg.m.rad^2	K_{F_4}	1.556×10^{-5}	kg.m.rad^2
K_{M_1}	3.965×10^{-7}	kg.m^2.rad^2	K_{M_2}	2.847×10^{-7}	kg.m^2.rad^2
K_{M_3}	4.404×10^{-7}	kg.m^2.rad^2	K_{M_4}	3.170×10^{-7}	kg.m^2.rad^2

TABLE II
DOB-BASED CONTROLLER PARAMETERS

Par.	Value	Par.	Value
M_{n_ζ}	diag$\{2, 2, 2, 0.5, 0.5, 0.5\}$	M_{n_σ}	diag$\{0.5, 0.5\}$
K_{P_ζ}	diag$\{3, 3, 10, 3, 3, 3\}$	K_{P_σ}	diag$\{10, 10\}$
K_{D_ζ}	diag$\{1.5, 1.5, 5, 3, 3, 3\}$	K_{D_σ}	diag$\{7, 7\}$
P	$[10\ 10\ 10\ 100\ 100\ 100\ 100\ 100]^T$		

to tune K_v, K_P, and K_D, such that the response speed of σ_b is much faster than that of ζ.

VII. SIMULATION STUDY

In this section, the previously proposed control strategy is simulated in MATLAB/SIMULINK program for the considered aerial manipulation system.

A. Simulation Environment

In order to make the simulation quite realistic, the following setup and assumptions have been made.

1) The model has been identified on the basis of real data through experimental tests. The identified parameters are given in Table I.
2) Linear and angular position and velocity of the quadrotor as well as the position and velocity of the manipulator joints are available at rate of 1 KHz.
3) A normally distributed measurement noise, with mean of 10^{-3} and standard deviation of 5×10^{-3}, has been added to the measured signals.
4) The controller outputs are computed at a rate of 1 KHz.
5) In order to test the robustness to the model uncertainties, a step disturbance is introduced, at instant 15 s, in the control matrix N (Actuators' losses), whose elements are assumed to be equal to 0.9 times their true values (i.e., 10% error). In addition, the end-effector has to pick a payload of value 200 g at instant 20 s and release it at 40 s.

B. Results and Discussion

Table II presents the controller parameter for the proposed control technique. Tuning of the controller parameters is carried out to maximize the speed of system response and minimize the tracking error. The reference trajectories for the end-effector are chosen such that the end-effector moves on a circular helix, while its orientation is fixed in a case and follows quintic polynomial trajectories in another case.

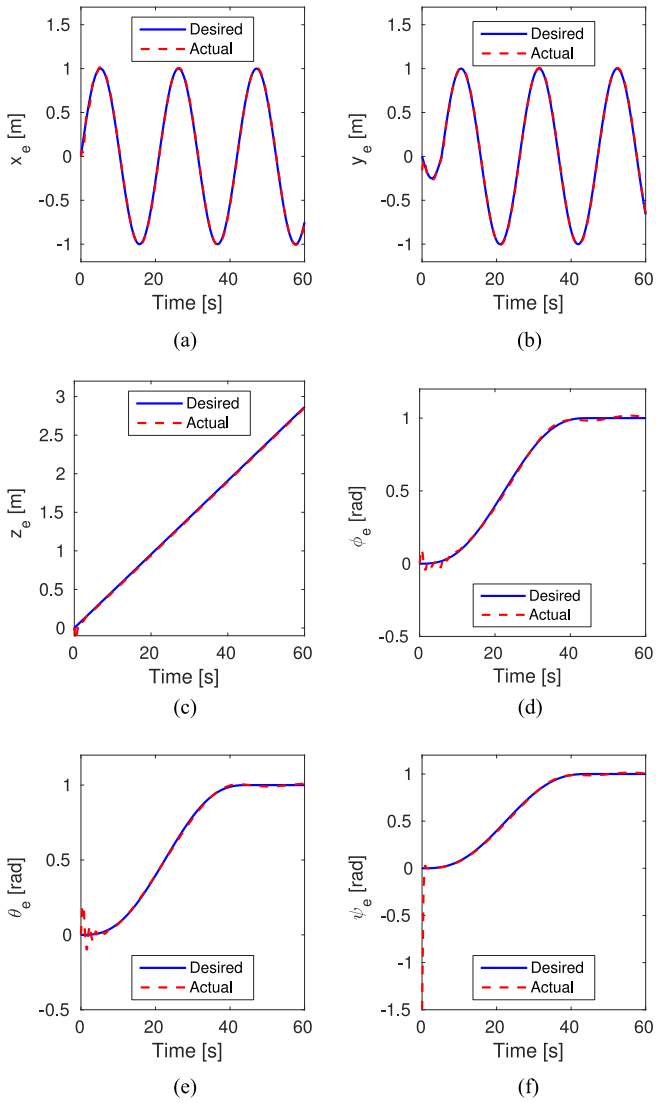

Fig. 8. Actual response of the end-effector pose (a) x_e, (b) y_e, (c) z_e, (d) ϕ_e, (e) θ_e, and (f) ψ_e.

The simulation results are presented in Figs. 8 and 9(a) (the marker represents the end-effector orientation; green, blue, and red for x-, y-, and z-axis). From these figures, it is possible to recognize that there are small oscillations after starting the system operation due to the time need to estimate the nonlinearities and disturbances. This time is about 4 s. After that period, the controller can quickly recover this error and provides good tracking of the desired trajectories. Moreover, it is clear that the capability of the controller to recover, with fast response (about 1 s), the tracking error due to the presence of the payload and the uncertainty in system parameters. Furthermore, Fig. 9(b) indicates that the required actuators efforts, which are the required thrust force from each rotor and the torque from each manipulator's

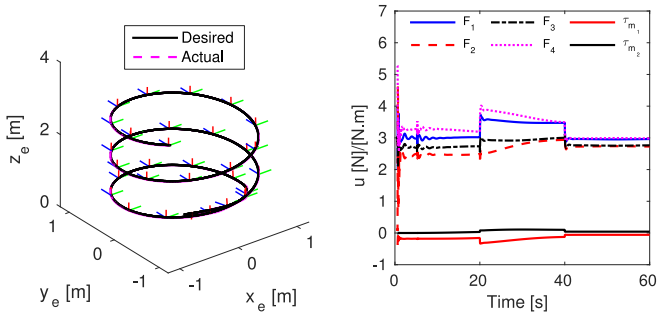

(a) (b)

Fig. 9. Three-dimensional trajectory and controller effort. (a) 3-D trajectory of end-effector with fixed orientation. (b) The required control efforts.

motor u are in the allowable limit. The maximum thrust force for each rotor is 6 N as obtained from the identification process, while the allowable input torque for the motor of joint 1 is 0.7 and 0.4 N·m for that of joint 2 as stated in the motors' data sheet. Therefore, one can contend that the control objectives are achieved by using this motion control scheme.

VIII. Conclusion

A new 6-DOF quadrotor-based aerial manipulator with minimum number of actuators is investigated. It provides solutions to the limitations found on the currently developed aerial manipulation systems by having maximum mobility with minimum weight. Description and design of the proposed system are introduced. Mathematical modeling are carried out. Proof that this system can perform any desired end-effector trajectory is done through analysis and numerical simulation of the complex inverse kinematics with nonholonomic constraints. A robust motion control scheme is designed and tested based on both the proposed inverse kinematics and the DOb technique in order to achieve 6-DOb task space trajectory tracking. Stability of the controller is analyzed. Simulation results enlighten the feasibility of the proposed system and the efficiency of the motion control scheme. As a future work, the proposed system will be tested experimentally.

References

[1] D. Mellinger, Q. Lindsey, M. Shomin, and V. Kumar, "Design, modeling, estimation and control for aerial grasping and manipulation," in *Proc. IEEE/RSJ Int. Conf. Intell. Robots Syst.*, 2011, pp. 2668–2673.

[2] Q. Lindsey, D. Mellinger, and V. Kumar, "Construction with quadrotor teams," *Auton. Robots*, vol. 33, no. 3, pp. 323–336, 2012.

[3] J. Willmann, F. Augugliaro, T. Cadalbert, R. D'Andrea, F. Gramazio, and M. Kohler, "Aerial robotic construction towards a new field of architectural research," *Int. J. Archit. Comput.*, vol. 10, no. 3, pp. 439–460, 2012.

[4] A. Albers, S. Trautmann, T. Howard, T. A. Nguyen, M. Frietsch, and C. Sauter, "Semi-autonomous flying robot for physical interaction with environment," in *Proc. IEEE Conf. Robot. Autom. Mechatronics*, 2010, pp. 441–446.

[5] M. Bisgaard, A. la Cour-Harbo, and J. Dimon Bendtsen , "Adaptive control system for autonomous helicopter slung load operations," *Control Eng. Pract.*, vol. 18, no. 7, pp. 800–811, 2010.

[6] N. Michael, J. Fink, and V. Kumar, "Cooperative manipulation and transportation with aerial robots," *Auton. Robots*, vol. 30, no. 1, pp. 73–86, 2011.

[7] F. A. Goodarzi, D. Lee, and T. Lee, "Geometric control of a quadrotor uav transporting a payload connected via flexible cable," *Int. J. Control, Autom. Syst.*, vol. 13, no. 6, pp. 1486–1498, 2015.

[8] F. A. Goodarzi and T. Lee, "Dynamics and control of quadrotor uavs transporting a rigid body connected via flexible cables," in *Proc. Amer. Control Conf.*, 2015, pp. 4677–4682.

[9] C. M. Korpela, T. W. Danko, and P. Y. Oh, "Mm-uav: Mobile manipulating unmanned aerial vehicle," *J. Intell. Robot. Syst.*, vol. 65, nos. 1–4, pp. 93–101, 2012.

[10] V. Lippiello and F. Ruggiero, "Cartesian impedance control of a uav with a robotic arm," in *Proc. 10th Int. IFAC Symp. Robot Control*, 2012, pp. 704–709.

[11] V. Lippiello and F. Ruggiero, "Exploiting redundancy in cartesian impedance control of uavs equipped with a robotic arm," in *Proc. IEEE/RSJ Int. Conf. Intell. Robots Systems*, 2012, pp. 3768–3773.

[12] M. Orsag, C. Korpela, and P. Oh, "Modeling and control of mm-uav: Mobile manipulating unmanned aerial vehicle," *J. Intell. Robot. Syst.*, vol. 69, nos. 1–4, pp. 227–240, 2013.

[13] S. Kim, S. Choi, and H. J. Kim, "Aerial manipulation using a quadrotor with a two dof robotic arm," in *Proc. IEEE/RSJ Int. Conf. Intell. Robots Syst.*, 2013, pp. 4990–4995.

[14] A. Khalifa, M. Fanni, A. Ramadan, and A. Abo-Ismail, "Modeling and control of a new quadrotor manipulation system," in *Proc. IEEE/RAS Int. Conf. Innov. Eng. Syst.*, 2012, pp. 109–114.

[15] A. Khalifa, M. Fanni, A. Ramadan, and A. Abo-Ismail, "Adaptive intelligent controller design for a new quadrotor manipulation system," in *Proc. IEEE Int. Conf. Syst., Man, Cybern.*, 2013, pp. 1666–1671.

[16] *Asctec Pelican Quadrotor*, Oct. 2014. [Online]. Available: http://www.asctec.de/en/uav-uas-drone-products/asctec-pelican/

[17] M. Achtelik, M. Achtelik, S. Weiss, and R. Siegwart, "Onboard imu and monocular vision based control for mavs in unknown in-and outdoor environments," in *Proc. IEEE Int. Conf. Robot. Autom.*, 2011, pp. 3056–3063.

[18] D. Zheng H. Wang, J. Wang, S. Chen, W. Chen, and X. Liang, "Image-based visual servoing of a quadrotor using virtual camera approach," *IEEE/ASME Trans. Mechatronics*, to be published, doi: 10.1109/TMECH.2016.2639531.

[19] I. Dryanovski, R. G. Valenti, and J. Xiao, "An open-source navigation system for micro aerial vehicles," *Auton. Robots*, vol. 34, no. 3, pp. 177–188, 2013.

[20] *LYNXMOTION*, Oct. 2014. [Online]. Available: http://www.lynxmotion.com/default.aspx

[21] M. W. Spong, S. Hutchinson, and M. Vidyasagar, *Robot Modeling and Control*, vol. 3. Hoboken, NJ: Wiley, 2006.

[22] B. K. Kim and W. K. Chung, "Performance tuning of robust motion controllers for high-accuracy positioning systems," *IEEE/ASME Trans. Mechatronics*, vol. 7, no. 4, pp. 500–514, Dec. 2002.

[23] S. Li, J. Yang, W.-h. Chen, and X. Chen, *Disturbance Observer-Based Control: Methods and Applications*. Boca Raton, FL, USA: CRC Press, 2014.

[24] E. Sariyildiz, H. Yu, K. Yu, and K. Ohnishi, "A nonlinear stability analysis for the robust position control problem of robot manipulators via disturbance observer," in *Proc. IEEE Int. Conf. Mechatronics*, 2015, pp. 28–33.

[25] K. S. Eom, I. H. Suh, and W. K. Chung, "Disturbance observer based path tracking control of robot manipulator considering torque saturation," *Mechatronics*, vol. 11, no. 3, pp. 325–343, 2001.

[26] H.-T. Choi, S. Kim, J. Choi, Y. Lee, T.-J. Kim, and J.-W. Lee, "A simplified model based disturbance rejection control for highly accurate positioning of an underwater robot," in *Proc. Oceans-St. John's, 2014*, 2014, pp. 1–5.

[27] P. J. From, J. T. Gravdahl, and K. Y. Pettersen, *Vehicle-Manipulator Systems*. New York, NY, USA: Springer, 2014.

[28] N. Sadegh and R. Horowitz, "Stability and robustness analysis of a class of adaptive controllers for robotic manipulators," *Int. J. Robot. Res.*, vol. 9, no. 3, pp. 74–92, 1990.

[29] R. Bickel and M. Tomizuka, "Passivity-based versus disturbance observer based robot control: Equivalence and stability," *J. Dyn. Syst., Meas. Control*, vol. 121, no. 1, pp. 41–47, 1999.

[30] P. A. Ioannou and J. Sun, *Robust Adaptive Control*. North Chelmsford, MA, USA: Courier Corp., 2012.

[31] Y.-C. Choi and H.-S. Ahn, "Nonlinear control of quadrotor for point tracking: Actual implementation and experimental tests," *IEEE/ASME Trans. Mechatronics*, vol. 20, no. 3, pp. 1179–1192, Jun. 2015.

Mohamed Fanni received the B.E. degree in mechanical engineering from the Faculty of Engineering, Cairo University, Giza, Egypt, in 1981; the M.Sc. degree in mechanical engineering from Mansoura University, Mansoura, Egypt, in 1986; and the Ph.D. degree in engineering from Karlsruhe University, Karlsruhe, Germany, in 1993.

He is an Associate Professor with the Egypt-Japan University of Science and Technology, New Borg El Arab, Egypt, on leave from the Production Engineering and Mechanical Design Department, Faculty of Engineering, Mansoura University. His major research interests include robotics engineering, automatic control, and mechanical design. His current research focuses on design and control of mechatronic systems, surgical manipulators, and flying/walking robots.

Ahmed Khalifa received the B.Sc. degree in industrial electronics and control engineering from Menoufia University, Al Minufya, Egypt, in 2009, and the M.Sc. and Ph.D. degrees in mechatronics and robotics engineering from Egypt-Japan University of Science and Technology, New Borg El Arab, Egypt, in 2013 and 2016, respectively.

He is currently with the Faculty of Electronic Engineering, Menofia University, as an Assistant Professor. His current research focuses on flying robots, multirobot systems, model-free robust and optimal control, and decentralized/cooperative control and state estimation.